actuators

MDPI

Article

Automatic Current-Constrained Double Loop ADRC for Electro-Hydrostatic Actuator Based on Singular Perturbation Theory

Rongrong Yang, Yongjie Ma, Jiali Zhao *, Ling Zhang and Hua Huang

School of Mechanical and Electrical Engineering, Lanzhou University of Technology, Lanzhou 730050, China
* Correspondence: j_l_zh@163.com; Tel.: +86-186-1046-0288

Abstract: For an electro-hydrostatic actuator (EHA), the position, speed, and current cascade three-loop control architecture are dominant in existing active disturbance rejection control (ADRC). However, this architecture suffers from many problems, such as severe noise sensitivity of the extended state observer (ESO), excessive complexity of control structure, and too many tuned parameters, which makes the controller not easy to implement in practice. Aiming at the above drawbacks, a novel cascade double-loop ADRC strategy that is automatic current-constrained is proposed, which makes the whole ADRC architecture simplified to the position and the integrated speed–current double-loop architecture. Firstly, for the position control loop, the singular perturbation theory is used to reasonably reduce the order of the model for the position subsystem of EHA. A reduced order ADRC controller (ROADRC) is synthesized, which not only effectively reduces the noise sensitivity of ESO, but also circumvents use of the actuation acceleration information in the controller design process. Secondly, the integrated speed–current ADRC controller is designed by taking the speed and current subsystems of EHA into synthesis, which avoids the problem of excessive current loop bandwidth in conventional three-loop control architecture, and the number of tuned parameters is significantly reduced. Additionally, an uncomplicated and effective automatic current-constrained ADRC controller (CACADRC) is designed to solve the problem in the integrated speed–current ADRC that the current cannot be automatically constrained. Finally, by comparing the three-loop PI controller with the traditional three-loop ADRC, a detailed simulation analysis is carried out to verify the effectiveness and merits of the proposed controller. The simulation results show that the proposed controller not only inherits the advantages of high precision and strong disturbance rejection performance of the conventional ADRC, but can also efficiently decrease the noise sensitivity of ESO and effectively achieve the current-constrained control.

Keywords: electro-hydrostatic actuator; active disturbance rejection control; singular perturbation theory; noise sensitivity; automatic current-constrained control

check for updates

Citation: Yang, R.; Ma, Y.; Zhao, J.; Zhang, L.; Huang, H. Automatic Current-Constrained Double Loop ADRC for Electro-Hydrostatic Actuator Based on Singular Perturbation Theory. *Actuators* **2022**, *11*, 381. https://doi.org/10.3390/act11120381

Academic Editors: Jean-Charles Mare and Jose Luis Sanchez-Rojas

Received: 6 November 2022
Accepted: 14 December 2022
Published: 17 December 2022

Publisher's Note: MDPI stays neutral with regard to jurisdictional claims in published maps and institutional affiliations.

Copyright: © 2022 by the authors. Licensee MDPI, Basel, Switzerland. This article is an open access article distributed under the terms and conditions of the Creative Commons Attribution (CC BY) license (https://creativecommons.org/licenses/by/4.0/).

1. Introduction

Electro-hydrostatic actuator (EHA) is a typical self-contained pump-controlled servo system, which has the preponderances of high integration, sizeable power-to-weight ratio, high reliability, high efficiency, and convenient installation and maintenance. It has been popular in many fields, such as main flight rudder control systems of more-electric aircraft, robots, vehicle active suspension devices, and injection molding machines [1–7]. However, EHA is a high-order complex nonlinear system with strong coupling to mechanical, electrical, and hydraulic. Moreover, there are a lot of parameter uncertainties and external disturbances in the system, which will degenerate the control performance of EHA. Therefore, a control strategy with high dynamic performance and strong robustness is urgently needed.

Currently, many advanced control methods have been extensively studied to improve the control performance of EHA. In [8], an adaptive backstepping control method was put

forward, which combines a special adaptive law with an improved backstepping algorithm to handle all uncertainties and nonlinearities in the EHA system. In [9], an asymptotically stable controller was presented based on a two-degree-of-freedom (2DOF) disturbance observer to compensate for the adverse effects of friction and internal leakage. A new adaptive damping variable sliding mode controller for EHA was developed to improve position step performance [10]. In [11], a composite adaptive control method based on a robust integral of the sign of error (RISE) was proposed, in which the parameter adaptive law was utilized to deal with unknown parameters, and RISE was adopted to repress the effects of the lumped disturbance on the system. To improve the position tracking performance of a novel EHA with a constant-torque variant-displacement pump, an adaptive control method combining backstepping and nonlinear projection was proposed in [12].

Recently, active disturbance rejection control (ADRC) has attracted more attention thanks to its strong robustness to uncertainties in the system [13,14]. ADRC is a 2DOF control method that does not completely lean upon the system model, which regards all kinds of uncertainties (parameter uncertainty, structural uncertainty, and external disturbance) in the system as a total disturbance, and the unique extended state observer (ESO) was utilized to real-time observe and compensate the total disturbance. At present, ADRC has been widely studied and applied in many fields, such as motor control, valve-controlled electro-hydraulic servo system, aircraft control, and robot control [15–21]. However, there is still very little ADRC research literature on EHA. A position and pressure cascade double-loop ADRC control architecture for single-rod EHA was proposed in [22], whereas this controller requires the pressure information of the hydraulic cylinder, and the dynamics of the motor's speed and current were neglected. The position, speed, and current cascade three-loop ADRC control structure were employed in [23]. Unfortunately, this method needs acceleration information in the design process of ADRC, which will lead to the oscillation of the control signal and even the system's instability due to the severe noise amplification effect of the acceleration signal. In [24], the position, pressure, speed, and current cascade four-loop control architecture was proposed, and ADRC was adopted for each control loop to improve the disturbance rejection ability, whereas this method requires the pressure information of the hydraulic cylinder two chambers and too many parameters need to be tuned. In addition, speed and current double-loop control architecture were adopted in [23,24]. Due to the excessive requirement on the bandwidth of the current loop, which results in employing power electronic devices with high operation frequency, then the hardware cost of the controller and the power consumption of power electronics were both increased.

For EHA, the existing ADRC control architecture often adopts the position, speed, and current cascaded three-loop ADRC control architecture, but this ADRC control architecture has the following defects: (1) the order of position loop ESO is 4 order, so ESO is very sensitive to noise, which makes it difficult for ESO to accurately estimate the disturbance; (2) in the design process of position loop ADRC, the acceleration information is required, and the acceleration information has an amplification effect on noise, which leads to control output oscillation and even system instability; (3) the speed and current are controlled by a cascaded double loop. As the current loop is the inner loop, the control bandwidth of the current loop required by the current loop is larger than that of the speed loop, which results in a larger switching frequency of the power electronic devices; (4) the position, speed, and current cascaded three-loop ADRC control structure is more complicated, and so many parameters need to be tuned, so it is not conducive to practical application in engineering. To solve these problems, this paper proposes a novel cascade double-loop ADRC method composed of the position loop and integrated speed–current loop based on singular perturbation theory. The main outstanding works of this paper are summarized as follows:

1. A novel cascade double-loop ADRC control architecture, including a reduced order position control loop and an integrated speed–current control loop, is presented,

which has a simpler structure and fewer tuning parameters compared with the existing architecture.

2. For the position control loop, a reduced-order ADRC controller (ROADRC) is synthesized based on singular perturbation theory. ROADRC does not need the acceleration information. Moreover, the noise sensitivity of ESO is significantly weakened. Hence, the control output signal of ROADRC is smoother, and the practical application difficulty of ROADRC is easier.
3. An effectively integrated speed–current ADRC with automatic current-constrained (CACADRC) is designed based on the barrier function. CACADRC not only solves the problem of excessive bandwidth of the current loop but also effectively solves the problem that the current cannot be constrained automatically after the integrated design. Furthermore, the detailed stability proof of CACADRC is given according to the Lyapunov theory.

2. System Description

2.1. Basic Principle

The basic schematic diagram of EHA is illustrated in Figure 1. It is primarily composed of a permanent magnet synchronous motor (PMSM), reversible plunger pump, check valves, relief valves, accumulator, mode switching valve, cylinder, sensors and drive controller, etc. Among them, the current sensor, resolver, and displacement sensor are responsible for measuring the current, speed of PMSM, and displacement of the piston rod, respectively. According to the desired position signal, the drive controller executes the corresponding control algorithm to generate the drive control signal to control the speed and direction of PMSM, and then control the output flow and pressure of the reversible piston pump to make the piston of the hydraulic cylinder perform telescopic movement, and finally realizes the control of the position, speed, and direction of the load. The accumulator fills the system with oil through check valve 1 or 2 to prevent the system from damaging the hydraulic components due to the "cavitation" phenomenon caused by the low oil pressure, and relief valve 1 or 2 is used to prevent the excessive high oil pressure of the system for safety.

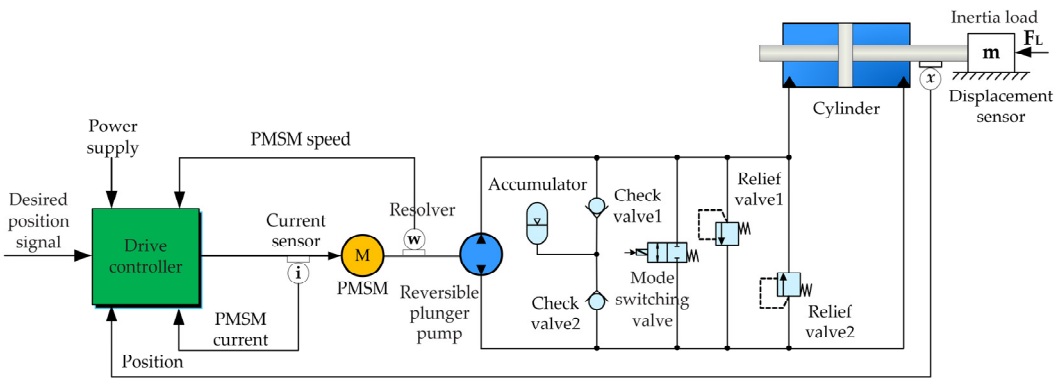

Figure 1. Schematic diagram of EHA.

2.2. Mathematical Modelling

2.2.1. Equations for Voltage and Motion of PMSM

Assuming the PMSM's rotor is surface-mounted, then the voltage equations of the q-axis and d-axis in the q, d rotor reference frame are mathematically depicted as:

$$\begin{cases} u_q = R_h i_q + L_q \dot{i}_q + p\omega_m (L_d i_d + \psi_f) \\ u_d = R_h i_d + L_d \dot{i}_d - p\omega_m L_q i_q \end{cases} \tag{1}$$

where u_q and u_d are q, d axis voltage components; R_h is the stator resistance; i_q and i_d are q, d axial current components; L_q and L_d are the equivalent inductance of q, d axis; ω_m is

the mechanical angular speed of PMSM; p is the number of pole pairs; and ψ_f is the flux linkage of the rotor permanent magnet.

The motion equation of the PMSM can be given by:

$$J_p\dot{\omega}_m = 1.5 \cdot p\psi_f i_q - B_p\omega_m - D_p(p_a - p_b) \tag{2}$$

where J_p is the rotor inertia of PMSM; B_p is the viscous friction coefficient of the reversible plunger pump; D_p is the displacement of the reversible plunger pump; and p_a and p_b are the oil outlet and inlet pressures of the pump, respectively.

2.2.2. Flow Equation of Reversible Plunger Pump

Regarding the reversible plunger pump, the flow equation can be described as follows:

$$\begin{cases} Q_a = D_p\omega_m - Q_{ip} - V_a\beta_e{}^{-1}\dot{p}_a - Q_{opa} \\ Q_b = D_p\omega_m - Q_{ip} + V_b\beta_e{}^{-1}\dot{p}_b + Q_{opb} \end{cases} \tag{3}$$

where Q_a and Q_b are the oil outlet and inlet flow of the pump, respectively; Q_{ip}, Q_{opa}, and Q_{opb} are the internal and external leakage flow of the pump, respectively; β_e is the effective oil bulk modulus; and V_a and V_b are respectively the volumes of oil outlet chamber and oil return chamber of the pump.

2.2.3. Flow Equation of Hydraulic Cylinder

Ignoring the external leakage flow of the hydraulic cylinder, the flow equation in two chambers of the hydraulic cylinder can be written as:

$$\begin{cases} Q_1 = A\dot{x} + \beta_e{}^{-1}(V_{10} + Ax)\dot{p}_1 + Q_{ic} \\ Q_2 = A\dot{x} - \beta_e{}^{-1}(V_{20} - Ax)\dot{p}_2 + Q_{ic} \end{cases} \tag{4}$$

where Q_1 and Q_2 are, respectively, the inflow and outflow flow of the two chambers of the hydraulic cylinder; A is the effective working area of the hydraulic cylinder piston; x is the displacement of the piston rod of the hydraulic cylinder; p_1 and p_2 are respectively the pressure of the two chambers of the hydraulic cylinder; Q_{ic} is the internal leakage flow in the hydraulic cylinder; and V_{10} and V_{20} are the volumes of the closed chamber on both sides of the hydraulic cylinder, respectively.

2.2.4. Motion Equation of the Hydraulic Cylinder

The balance equation that denotes the connection between the load and the output force of the hydraulic cylinder can obtain the following:

$$m_t\ddot{x} = A(p_1 - p_2) - B_t\dot{x} - F_L \tag{5}$$

where m_t is the total mass of the piston, piston rod, and load; B_t is the total viscous friction coefficient of the hydraulic cylinder and the load; and FL is the external load force applied to the piston rod.

2.2.5. Equation of Pressure Dynamics

According to the flow continuity characteristics, the flow equation can be written as follows:

$$\begin{cases} Q_a = Q_1 + Q_{c1} - Q_{r1} \\ Q_b = Q_2 + Q_{c2} - Q_{r2} \end{cases} \tag{6}$$

where Q_{c1}, Q_{c2}, Q_{r1}, and Q_{r2} are the flow through the check valve and the relief valve, respectively.

Assuming that the pressure loss from the pump to the hydraulic cylinder line is zero because the flow channel in the valve block is very short, then $p_a = p_1$, $p_b = p_2$. In addition,

$V_a = V_{10} + Ax$, $V_b = V_{20} - Ax$, considering Equations (3), (4), and (6), we can obtain the following:

$$\begin{cases} \dot{p}_1 = (\beta_e/2) \cdot (V_{10} + Ax)^{-1}(D_p\omega_m - A\dot{x} - Q_{ip} - Q_{ic} - Q_{opa} + Q_{v1}) \\ \dot{p}_2 = (\beta_e/2) \cdot (V_{20} + Ax)^{-1}(-D_p\omega_m + A\dot{x} + Q_{ip} + Q_{ic} - Q_{opb} - Q_{v2}) \end{cases} \tag{7}$$

where $Q_{v1} = -Q_{c1} + Q_{r1}$; $Q_{v2} = -Q_{c2} + Q_{r2}$.

Assuming that the piston is in the middle position of the hydraulic cylinder at the initial stage, namely $V_{10} \approx V_{20} = V_0$, and considering that the hydraulic cylinder is symmetric, it is approximately $\dot{p}_1 = -\dot{p}_2$. Equation (7) is taken into consideration to obtain:

$$\dot{p}_L = \dot{p}_1 - \dot{p}_2 = \beta_e V_0^{-1}[D_p\omega_m - A\dot{x} - Q_{ip} - Q_{ic} + Q_{un}] = \beta_e V_0^{-1}[D_p\omega_m - A\dot{x} - C_t p_L + Q_{un}] \tag{8}$$

where $p_L = p_1 - p_2$ is the load pressure; C_t is the total leakage coefficient of the pump and the hydraulic cylinder; and $Q_{un} = -(Q_{opa} - Q_{opb})/2 + (Q_{v1} + Q_{v2})/2$.

Defining state variables as $\mathbf{X} = (x_1, x_2, x_3, x_4, x_5, x_6)^T = (x, \dot{x}, p_L, \omega_m, i_q, i_d)^T$, the state equation of EHA can be depicted as follows:

$$\begin{cases} \dot{x}_1 = x_2 \\ \dot{x}_2 = m_t^{-1}(Ax_3 - B_t x_2 + d_{Lm}) \\ \dot{x}_3 = \beta_e V_0^{-1}(D_p x_4 - Ax_2 - C_t x_3 + Q_{un}) \\ \dot{x}_4 = J_p^{-1}\left(1.5 \cdot p\psi_f x_5 - B_p x_4 + d_{Lp}\right) \\ \dot{x}_5 = L_q^{-1}\left[-R_h x_5 - p x_4(L_d x_6 + \psi_f) + u_q\right] \\ \dot{x}_6 = L_d^{-1}\left[-R_h x_6 + p x_4 L_q x_5 + u_d\right] \end{cases} \tag{9}$$

where $d_{Lm} = -F_L$; $d_{Lp} = -D_p p_L$.

With u_d, u_q as the direct control quantity, EHA is a 5-order, 2-input single-output system. For the purpose of simplifying the controller design process, the whole system is divided into three subsystems; namely, the position subsystem composed of state variables x, $\dot{x}$, p_L, the speed subsystem composed of state variable ω_m, and the current subsystem composed of state variables i_d, i_q.

2.3. Reduced Order Model of EHA Based on Singular Perturbation Theory

Because the design order of position loop ESO in the conventional three-loop ADRC architecture of EHA is 4 order and the acceleration information in the controller has an amplification effect on noise, ESO is very sensitive to noise. Therefore, if the position loop ESO can be reduced-order processed, the practicability of the position loop ADRC controller will be significantly increased. Based on the above idea, the singular perturbation theory is utilized to reduce the order of the position subsystem. First, the position subsystem is written into the singular perturbation form, and then the order of the position subsystem model is reduced [25].

It is noted that the effective oil bulk modulus β_e is a numerically sizeable physical quantity in Equation (8); usually, its value is (7~15) $\times 10^8$ Pa, so $\varepsilon_s = \beta_e^{-1} V_0$ is chosen as the singular perturbation parameter. Defining the state variables $\mathbf{X}_s = (x, \dot{x})^T$ and $Z_s = p_L$, Equations (5) and (8) can be written in the singularly perturbed standard form:

$$\begin{cases} \ddot{x} = m_t^{-1}Ap_L - m_t^{-1}F_L - m_t^{-1}B_t\dot{x} \\ \varepsilon_s\dot{p}_L = D_p\omega_m - A\dot{x} - C_t p_L + Q_{un} \end{cases} \tag{10}$$

Let $\varepsilon_s = 0$, the following formula of Equation (10) can degenerate into an algebraic equation:

$$0 = D_p\omega_m - A\dot{x} - C_t p_L + Q_{un} \tag{11}$$

The quasi-steady state quantity $\overline{p}_L$ of p_L can be obtained as follows:

$$\overline{p}_L = C_t^{-1}(D_p\omega_m - A\dot{x} + Q_{un}) \tag{12}$$

Define $y_\tau = p_L - \overline{p}_L$, then:

$$\begin{aligned} \varepsilon_s\dot{y}_\tau &= \varepsilon_s\dot{p}_L - \varepsilon_s\dot{\overline{p}}_L \\ &= D_p\omega_m - A\dot{x} - C_t p_L - \varepsilon_s\dot{\overline{p}}_L \\ &= C_t\overline{p}_L - C_t p_L - \varepsilon_s\dot{\overline{p}}_L \\ &= -C_t y_\tau - \varepsilon_s\dot{\overline{p}}_L \end{aligned} \tag{13}$$

Set $\varepsilon_s = 0$, $\tau_s = t/\varepsilon_s$, then Equation (13) can be converted into the new timescale τ_s framework, then the boundary layer model equation can obtain the following:

$$\frac{dy_\tau}{d\tau_s} = -C_t y_\tau \tag{14}$$

It is clear that the boundary layer model is asymptotically stable concerning the equilibrium point $y_\tau = 0$. According to Tikhonov theorem, it can be known that:

$\forall\varepsilon_s{}^*, \varepsilon_s{}^{**} \in \mathbf{R}^+$, when ε_s satisfies $\varepsilon_s{<}\varepsilon_s{}^{**}{<}\varepsilon_s{}^*$, we have $x - \overline{x} = O(\varepsilon_s), \dot{x} - \dot{\overline{x}} = O(\varepsilon_s)$ for $t \in [t_0, \infty]$, and we have $p_L - \overline{p}_L = O(\varepsilon_s)$ for $t \in [t_b, \infty]$.

The quasi-steady state quantity $\overline{p}_L$ is substituted into the upper formula of Equation (10), and the reduced order model can be obtained as follows:

$$\begin{aligned} \ddot{x} &= m_t^{-1}A\overline{p}_L - m_t^{-1}B_t\dot{x} - m_t^{-1}F_L \\ &= AD_p(m_tC_t)^{-1}\omega_m - A^2(m_tC_t)^{-1}\dot{x} + A(m_tC_t)^{-1}Q_{un} - m_t^{-1}B_t\dot{x} - m_t^{-1}F_L \end{aligned} \tag{15}$$

Define the state variables $\mathbf{X} = (x_1, x_2)^T = (x, \dot{x})^T$, then Equation (15) can be written as the following state space form:

$$\begin{cases} \dot{x}_1 = x_2 \\ \dot{x}_2 = g_{x0}\omega_m + d_x \end{cases} \tag{16}$$

where g_{x0} is the nominal value of $g_x = AD_p/(m_tC_t)$; $d_x = \Delta g_x\omega_m - [A^2(m_tC_t)^{-1} + m_t{}^{-1}B_t]\cdot\dot{x} + A(m_tC_t)^{-1}Q_{un} - m_t{}^{-1}F_L$; and Δg_x is the perturbation value of parameter g_x.

3. Design of Novel ADRC for EHA

If the two-position two-way mode switching valve in Figure 1 is closed, then the system is in position control mode. The EHA control architecture diagram of the proposed method is shown in Figure 2.

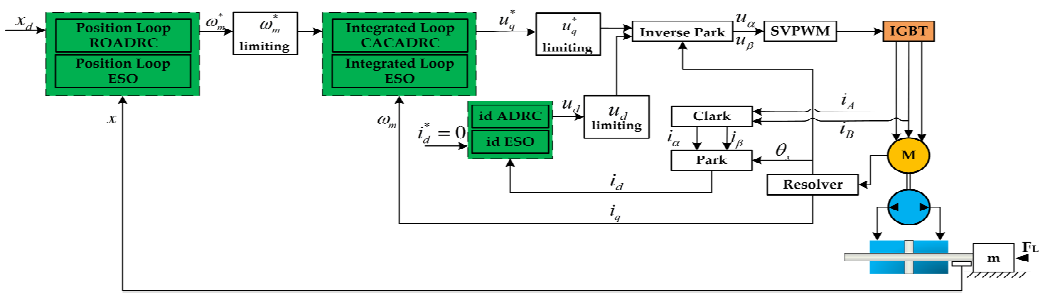

Figure 2. The control architecture diagram of the EHA.

While the two-position two-way mode switching valve is switched on, the system is in speed control mode. The position loop in Figure 2 is removed to obtain the EHA control architecture diagram of the CACADRC.

3.1. ROADRC Design

By designing ESO to accurately estimate d_x, converting it into a corresponding control quantity to cancel the disturbance, and then considering it as a nominal model without any disturbance to design the controller, the difficulty of controller design will be significantly reduced.

Assuming that ω_{mc} represents the disturbance compensation control quantity and ω_{m0} represents the nominal control quantity, then the output of the ROADRC controller is $\omega_m{}^* = \omega_{m0} + \omega_{mc}$.

In the following, ESO is designed to estimate d_x, and the total disturbance d_x is expanded into an additional state denoted by x_3, and its derivative satisfies this condition: $\dot{d}_x = h_x$. Then, the ESO can be constructed as:

$$\begin{cases} \dot{\hat{x}}_1 = \hat{x}_2 + l_{x1}(x_1 - \hat{x}_1) \\ \dot{\hat{x}}_2 = g_{x0}\omega_m + \hat{x}_3 + l_{x2}(x_1 - \hat{x}_1) \\ \dot{\hat{x}}_3 = l_{x3}(x_1 - \hat{x}_1) \end{cases} \tag{17}$$

where l_{x1}, l_{x2} and $l_{x3} > 0$ are satisfying the Hurwitz condition, and $\hat{x}_1$, $\hat{x}_2$ and $\hat{x}_3$ are the estimated values of x_1, x_2, and x_3, respectively.

Then, $\omega_m{}^*$ can be designed as:

$$\omega_m^* = g_{x0}^{-1}[\ddot{x}_d + k_{x1}(x_d - \hat{x}_1) + k_{x2}(\dot{x}_d - \hat{x}_2) - \hat{x}_3] \tag{18}$$

where x_d is the position reference, and k_{x1} and k_{x2} are the control parameters of ROADRC.

It can be seen from Equation (17) that three parameters $l_{x1} \sim l_{x3}$ need to be tuned, and the characteristic equation $s^3 + l_{x1}s^2 + l_{x2}s + l_{x3}$ of ESO can be integrated into the mode of multiple poles, namely $(s + \omega_{ox})^3$. In this way, $l_{x1} \sim l_{x3}$ is only related to the ESO bandwidth ω_{ox}, so ESO only needs to set one parameter ω_{ox}. Then, $l_{x1} \sim l_{x3}$ can be easily calculated as [26]:

$$l_{x1} = 3\omega_{ox}, l_{x2} = 3\omega_{ox}^2, l_{x3} = \omega_{ox}^3 \tag{19}$$

Similarly, the control system is of order 2, and the characteristic equation $s^2 + k_{x2}s + k_{x1}$ is integrated into the mode of multiple poles, namely $(s + \omega_{cx})^2$. ω_{cx} is the control bandwidth, so one only needs to adjust the ω_{cx} parameter. In this case, $k_{x1} \sim k_{x2}$ can be easily calculated as:

$$k_{x2} = 2\omega_{cx}, k_{x1} = \omega_{cx}^2 \tag{20}$$

3.2. CACADRC Design

In conventional three-loop control architecture, the bandwidth of the current loop is usually required to be larger than that of the speed loop, so it requires a higher operating frequency of power electronic devices, which leads to the increase in the hardware cost of the controller and the power consumption of power electronics. Moreover, this architecture needs to set more parameters. To deal with these problems, the speed loop, and current loop can be regarded as a whole to design the controller.

Rewrite motor motion Equation (2) as follows:

$$\begin{aligned} \dot{\omega}_m &= g_\omega i_q - J_p{}^{-1}B_p\omega_m - J_p{}^{-1}D_p p_L \\ &= g_\omega i_q + a_\omega \end{aligned} \tag{21}$$

where $a_\omega = -J_p{}^{-1}B_p\omega_m - J_p{}^{-1}D_pP_L$.

By taking the derivative of both sides of Equation (21) and considering Equation (1), it can be obtained:

$$\begin{aligned}\ddot{\omega}_m &= g_\omega \dot{i}_q + \dot{a}_\omega \\ &= g_\omega[L_q{}^{-1}u_q - L_q{}^{-1}R_h i_q - L_q{}^{-1}p\omega_m(L_q i_d + \psi_f)] + \dot{a}_\omega \\ &= g_{\omega q}u_q + g_\omega[-L_q{}^{-1}R_h i_q - L_q{}^{-1}p\omega_m(L_d i_d + \psi_f)] + \dot{a}_\omega \\ &= g_{\omega q0}u_q + \triangle g_{\omega q}u_q + g_\omega[-L_q{}^{-1}R_h i_q - L_q{}^{-1}p\omega_m(L_d i_d + \psi_f)] + \dot{a}_\omega \\ &= g_{\omega q0}u_q + d_{\omega q}\end{aligned} \tag{22}$$

where $g_{\omega q0}$ is the nominal value of $g_{\omega q} = 3/2 \cdot p\psi_f J_p{}^{-1}L_q{}^{-1}$; $d_{\omega q} = \Delta g_{\omega q}u_q + g_\omega[-L_q{}^{-1}R_h i_q - L_q{}^{-1} p\omega_m(L_d i_d + \psi_f)] + \dot{a}_\omega$, and $\Delta g_{\omega q}$ is the perturbation value of parameter $g_{\omega q}$.

Defining the state variables $\omega_m = (\omega_{m1}, \omega_{m2})^T = (\omega_m, \dot{\omega}_m)^T$ and rewriting Equation (22) as the following state space form:

$$\begin{cases} \dot{\omega}_{m1} = \omega_{m2} \\ \dot{\omega}_{m2} = g_{\omega q0}u_q + d_{\omega q} \end{cases} \tag{23}$$

Assuming that u_{qc} represents the disturbance compensation control quantity and u_{q0} represents the nominal control quantity, the output of the integrated speed–current control is $u_{qi}{}^* = u_{q0} + u_{qc}$.

In the following, ESO is designed to estimate $d_{\omega q}$, and the total disturbance $d_{\omega q}$ is expanded into a state, namely $\omega_{m3} = d_{\omega q}$, denoted as $\dot{d}_{\omega q} = h_{\omega q}$, ESO needs to be designed as order 3, and the ESO is constructed as:

$$\begin{cases} \dot{\hat{\omega}}_{m1} = \hat{\omega}_{m2} + l_{\omega q1}(\omega_{m1} - \hat{\omega}_{m1}) \\ \dot{\hat{\omega}}_{m2} = g_{\omega q0}u_q + \hat{\omega}_{m3} + l_{\omega q2}(\omega_{m1} - \hat{\omega}_{m1}) \\ \dot{\hat{\omega}}_{m3} = l_{\omega q3}(\omega_{m1} - \hat{\omega}_{m1}) \end{cases} \tag{24}$$

where $l_{\omega q1}$, $l_{\omega q2,}$ and $l_{\omega q3} > 0$ are satisfying Hurwitz condition, and $\hat{\omega}_{m1}$, $\hat{\omega}_{m2}$ and $\hat{\omega}_{m3}$ are the estimated values of ω_{m1}, $\omega_{m2,}$ and ω_{m3}, respectively.

Defining the speed tracking error is as $e_{\omega q1} = \omega_{md} - \hat{\omega}_{m1}$, $e_{\omega q2} = \dot{\omega}_{md} - \hat{\omega}_{m2}$, then $u_{qi}{}^*$ is designed as:

$$u_{qi}^* = g_{\omega q0}^{-1}(\ddot{\omega}_{md} + k_{\omega q1}e_{\omega q1} + k_{\omega q2}e_{\omega q2} - \hat{\omega}_{m3}) \tag{25}$$

where ω_{md} is the speed reference, and $k_{\omega q1}$ and $k_{\omega q2}$ are the control parameters of the integrated speed–current loop controller.

However, it should be noted that after the integration of ω_m and i_q is processed, i_q is in an uncontrollable state, which means the amplitude of i_q cannot be limited as the traditional ADRC architecture; namely, i_q may be larger than i_{qmax}. To deal with this problem, a CACADRC controller that can automatically constrain i_q is developed here. Therefore, Equation (25) is amended as follows:

$$u_q^* = g_{\omega q0}^{-1}[\ddot{\omega}_{md} + k_{\omega q1}e_{\omega q1} + (k_{\omega q2} + f_{br})e_{\omega q2} - \hat{\omega}_{m3}] \tag{26}$$

where $f_{br} = \frac{l}{\tan^{-1}(i_{qmax}^2 - i_q^2)}$ is the barrier function; l is the current penalty coefficient; and i_{qmax} is the limiting value of i_q.

Remark 1: *The differential term $e_{\omega q2}$ of speed tracking error $e_{\omega q1}$ characterizes the damping or angular acceleration of the system to some extent. The larger the damping is, the slower the tracking speed of the rotating speed is, but the more stable the tracking transient is. As can be seen from Figure 3, when i_q approaches i_{qmax}, the nonlinear current penalty term increases, the damping of the system increases, and the angular acceleration decreases. It is noted that the angular acceleration is proportional to the current, so i_q decreases. As i_q moves away from i_{qmax}, the nonlinear current penalty term decreases, the damping of the system decreases, the angular acceleration increases, and i_q begins to increase again. Finally, i_q fluctuates around i_{qmax}.*

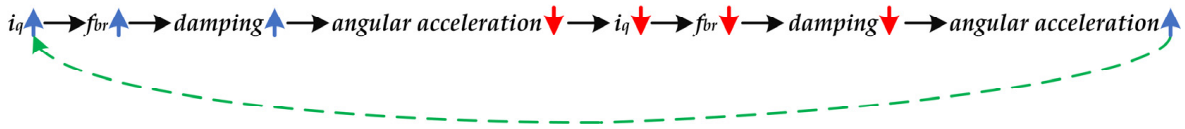

Figure 3. Automatic current-constrained mechanism of barrier function f_{br}.

The ESO bandwidth of CACADRC is represented by $\omega_{o\omega q}$. At the same time, since the ESO of CACADRC is also of order 3, similar to the ESO's parameter tuning process of the position loop, $l_{\omega q1} \sim l_{\omega q3}$ can be easily calculated as:

$$l_{\omega q1} = 3\omega_{o\omega q}, l_{\omega q2} = 3\omega_{o\omega q}^2, l_{\omega q3} = \omega_{o\omega q}^3 \tag{27}$$

The control system is of order 2, and the control bandwidth of CACADRC is $\omega_{c\omega q}$. In this case, it is easy to calculate $k_{\omega q1} \sim k_{\omega q2}$ as:

$$k_{\omega q2} = 2\omega_{c\omega q}, k_{\omega q1} = \omega_{c\omega q}^2 \tag{28}$$

4. Stability Proof of the System

4.1. Stability Proof of ROADRC

4.1.1. Proof of Convergence of ESO

Considering Equation (17), then the characteristic polynomial of ROADRC's ESO is denoted by:

$$\lambda(s) = s^3 + l_{x1}s^2 + l_{x2}s + l_{x3} = (s + \omega_{ox})^3 \tag{29}$$

where $\omega_{ox} > 0$, according to the binomial theorem:

$$l_{xi} = \frac{(n+1)!}{i!(n+1-i)!}\omega_{ox}^i = \alpha_i\omega_{ox}^i, i = 1, 2, 3. \tag{30}$$

Let $e_i = x_i - \hat{x}_i$, $i = 1, 2, 3$, subtract Equation (17) from Equation (16), and we have:

$$\begin{cases} \dot{e}_1 = e_2 - l_{x1}e_1 \\ \dot{e}_2 = e_3 - l_{x2}e_1 \\ \dot{e}_3 = h_x - l_{x3}e_1 \end{cases} \tag{31}$$

Substituting Equation (30) into Equation (31), we can obtain:

$$\begin{cases} \dot{e}_1 = e_2 - \alpha_1\omega_{ox}e_1 \\ \dot{e}_2 = e_3 - \alpha_2\omega_{ox}^2e_1 \\ \dot{e}_3 = h_x - \alpha_3\omega_{ox}^3e_1 \end{cases} \tag{32}$$

Make $\varepsilon_i = e_i/{\omega_{ox}}^{i-1}$, $i = 1, 2, 3$, then:

$$\begin{cases} \dot{\varepsilon}_1 = \omega_{ox}\varepsilon_2 - \alpha_1\omega_{ox}\varepsilon_1 \\ \dot{\varepsilon}_2 = \omega_{ox}\varepsilon_3 - \alpha_2\omega_{ox}\varepsilon_1 \\ \dot{\varepsilon}_3 = h_x/\omega_{ox}^2 - \alpha_3\omega_{ox}\varepsilon_1 \end{cases} \tag{33}$$

Writing the above equation in matrix form:

$$\dot{\boldsymbol{\varepsilon}} = \omega_{ox}\mathbf{A}\boldsymbol{\varepsilon} + \frac{\mathbf{B}h_x}{\omega_{ox}^2} \tag{34}$$

where $\mathbf{A} = \begin{pmatrix} -\alpha_1 & 1 & 0 \\ -\alpha_2 & 0 & 1 \\ -\alpha_3 & 0 & 0 \end{pmatrix}$, $\boldsymbol{\varepsilon} = \begin{pmatrix} \varepsilon_1 & \varepsilon_2 & \varepsilon_3 \end{pmatrix}^T$, $\mathbf{B} = \begin{pmatrix} 0 & 0 & 1 \end{pmatrix}^T$.

Since **A** satisfies Hurwitz's condition, there exists a positive definite matrix **P**, such that $\mathbf{A}^T\mathbf{P} + \mathbf{PA} = -\mathbf{I}$. Defining the Lyapunov function $V(\boldsymbol{\varepsilon}) = \boldsymbol{\varepsilon}^T\mathbf{P}\boldsymbol{\varepsilon}$, and taking the derivative about time:

$$\begin{aligned}\dot{V}(\boldsymbol{\varepsilon}) &= \dot{\boldsymbol{\varepsilon}}^T\mathbf{P}\boldsymbol{\varepsilon} + \boldsymbol{\varepsilon}^T\mathbf{P}\dot{\boldsymbol{\varepsilon}} \\ &= (\boldsymbol{\varepsilon}^T\mathbf{A}^T\omega_{ox}^T + \mathbf{B}^T h_x/\omega_{ox}^2)\mathbf{P}\boldsymbol{\varepsilon} + \boldsymbol{\varepsilon}^T\mathbf{P}(\omega_{ox}\mathbf{A}\boldsymbol{\varepsilon} + \mathbf{B}h_x/\omega_{ox}^2) \\ &= \boldsymbol{\varepsilon}^T(\mathbf{A}^T\omega_{ox}^T\mathbf{P} + \mathbf{P}\omega_{ox}\mathbf{A})\boldsymbol{\varepsilon} + 2\mathbf{B}^T h_x/\omega_{ox}^2\mathbf{P}\boldsymbol{\varepsilon} \\ &= -\|\boldsymbol{\varepsilon}\|^2 + 2\|\mathbf{PB}\|(h_x/\omega_{ox}^2)\|\boldsymbol{\varepsilon}\| \\ &\le -\|\boldsymbol{\varepsilon}\|(\|\boldsymbol{\varepsilon}\| - 2\|\mathbf{PB}\|h_x/\omega_{ox}^2)\end{aligned} \tag{35}$$

If h_x is bounded, i.e., $|h_x| < M$, when $\|\boldsymbol{\varepsilon}\| > 2\|\mathbf{PB}\|h_x/\omega_{ox}^2$, $\dot{V}(\varepsilon) < 0$ is always satisfied, then $\|\varepsilon\|$ will converge to the range $\|\varepsilon\| \le 2\|\mathbf{PB}\|h_x/\omega_{ox}^2$, so $\|\varepsilon\|$ is bounded. Considering $\varepsilon_i = e_i/{\omega_{ox}}^{i-1}$, $i = 1, 2, 3$, and inequality (35), we can obtain the following:

$$\|e_i\| \le 2\|\mathbf{PB}\|h_x/\omega_{ox}^{3-i}, i = 1, 2, 3 \tag{36}$$

Thus, $\|\mathbf{e}\|$ is bounded. In particular, when $h_x = 0$, **e** is asymptotically stable, namely $\lim\limits_{t\to\infty}\mathbf{e} = 0$.

4.1.2. Stability Proof of Controller

Substituting Equation (18) into Equation (16), we can obtain:

$$\begin{aligned}\ddot{x}_1 &= g_{x0}\omega_m + d_x = \ddot{x}_d + k_{x1}(x_d - \hat{x}_1) + k_{x2}(\dot{x}_d - \hat{x}_2) + (d_x - \hat{x}_3) \\ &= \ddot{x}_d + k_{x1}[x_d - (x_1 - \overline{x}_1)] + k_{x2}\left[\dot{x}_d - (x_2 - \overline{x}_2)\right] + \overline{d}_x \\ &= \ddot{x}_d + k_{x1}e + k_{x2}\dot{e} + k_{x1}\overline{x}_1 + k_{x2}\overline{x}_2 + \overline{d}_x\end{aligned} \tag{37}$$

Rearranging Equation (37), we have:

$$\ddot{e} + k_{x2}\dot{e} + k_{x1}e = -k_{x2}\overline{x}_2 - k_{x1}\overline{x}_1 - \overline{d}_x \tag{38}$$

Writing the above equation in matrix form:

$$\dot{\mathbf{E}} = \mathbf{A}_x\mathbf{E} - \mathbf{K}_x\overline{\mathbf{X}} \tag{39}$$

where $\mathbf{E} = (e, \dot{e})^T$, $\mathbf{A}_x = \begin{pmatrix} 0 & 1 \\ -k_{x1} & -k_{x2} \end{pmatrix}$, $\mathbf{K}_x = (k_{x1}, k_{x2}, 1)$, $\overline{\mathbf{X}} = \left(\overline{x}_1, \overline{x}_2, \overline{d}_x\right)^T$.

Since k_{x1} and k_{x2} satisfy Hurwitz's condition, there exists a positive definite matrix $\mathbf{P}_x$, such that $\mathbf{A}_x^T\mathbf{P}_x + \mathbf{P}_x\mathbf{A}_x = -\mathbf{I}$. Defining the Lyapunov function $V = \mathbf{E}^T\mathbf{P}_x\mathbf{E}$, taking the derivative of V about time:

$$\begin{aligned}\dot{V} &= \dot{\mathbf{E}}^T\mathbf{P}_x\mathbf{E} + \mathbf{E}^T\mathbf{P}_x\dot{\mathbf{E}} \\ &= \left(\mathbf{E}^T\mathbf{A}_x^T - \overline{\mathbf{X}}^T\mathbf{K}_x^T\right)\mathbf{P}_x\mathbf{E} + \mathbf{E}^T\mathbf{P}_x\left(\mathbf{A}_x\mathbf{E} - \mathbf{K}_x\overline{\mathbf{X}}\right) \\ &= \mathbf{E}^T\mathbf{A}_x^T\mathbf{P}_x\mathbf{E} + \mathbf{E}^T\mathbf{P}_x\mathbf{A}_x\mathbf{E} - \overline{\mathbf{X}}^T\mathbf{K}_x^T\mathbf{P}_x\mathbf{E} - \mathbf{E}^T\mathbf{P}_x\mathbf{K}_x\overline{\mathbf{X}} \\ &= \mathbf{E}^T\left(\mathbf{A}_x^T\mathbf{P}_x + \mathbf{P}_x\mathbf{A}_x\right)\mathbf{E} - 2\mathbf{E}^T\mathbf{P}_x\mathbf{K}_x\overline{\mathbf{X}} \\ &= -\|\mathbf{E}\|^2 - 2\mathbf{E}^T\mathbf{P}_x\mathbf{K}_x\overline{\mathbf{X}}\end{aligned} \tag{40}$$

$$\begin{aligned}&\le -\|\mathbf{E}\|^2 + 2\breve{}_{\max}(\mathbf{P}_x)\|\mathbf{E}\|\|\mathbf{K}_x\|\left\|\overline{\mathbf{X}}\right\| \\ &= -\|\mathbf{E}\|\left(\|\mathbf{E}\| - 2\breve{}_{\max}(\mathbf{P}_x)\|\mathbf{K}_x\|\left\|\overline{\mathbf{X}}\right\|\right)\end{aligned} \tag{41}$$

where λ_{max} $(\mathbf{P}_x)$ is the largest eigenvalue of $\mathbf{P}_x$.

When $\|\mathbf{E}\| > 2\breve{}_{\max}(\mathbf{P}_x)\|\mathbf{K}_x\|\left\|\overline{\mathbf{X}}\right\|$, $\dot{V} < 0$ is always satisfied, then $\|\mathbf{E}\|$ must converge to the range $\|\mathbf{E}\| \leq 2\breve{}_{\max}(\mathbf{P}_x)\|\mathbf{K}_x\|\left\|\overline{\mathbf{X}}\right\|$, i.e., $\|\mathbf{E}\|$ is bounded. Especially when the ESO estimation error is $\left\|\overline{\mathbf{X}}\right\| \to 0$, $\dot{V} \leq -\|\mathbf{E}\|^2 < 0$, then $\|\mathbf{E}\| \to 0$.

4.2. Stability Proof of CACADRC

4.2.1. Proof of Convergence of ESO

The proof process of ESO convergence is similar to that of position loop ESO.

4.2.2. Stability Proof of Controller

Combined with Equations (23) and (26), the closed-loop system can be given as:

$$\begin{cases} \dot{\omega}_{m1} = \omega_{m2} \\ \dot{\omega}_{m2} = \ddot{\omega}_{md} + k_{\omega q1}e_{\omega q1} + k_{\omega q2}e_{\omega q2} + l/\tan^{-1}(i_{qmax}^2 - i_q^2)e_{\omega q2} + \overline{d}_{\omega q} \end{cases} \tag{42}$$

Therefore, the control system can be written as follows:

$$\begin{cases} \dot{e}_{\omega q1} = e_{\omega q2} \\ \dot{e}_{\omega q2} = -k_{\omega q1}e_{\omega q1} - k_{\omega q2}e_{\omega q2} - l/\tan^{-1}(i_{qmax}^2 - i_q^2)e_{\omega q2} - \overline{d}_{\omega q} \end{cases} \tag{43}$$

Theorem 1. *If the initial value $i_q(0) \in (-i_{qmax}, i_{qmax})$, (e_{wq1}, e_{wq2}) asymptotically converges to a bounded closed set $\Omega_E = \left\{e_{\omega q}\middle|\beta_{k\omega q}V(e_{\omega q}) \leq \frac{1}{2}\overline{d}_{\omega q}^2\right\}$, where $\beta_{k\omega q}$ is indicated below. In the meantime, $i_q(t) \in (-i_{qmax}, i_{qmax})$ always hold.*

Proof: The Lyapunov function is defined as:

$$V(e_{\omega q}) = \frac{1}{2}e_{\omega q1}^2 + \frac{1}{2}e_{\omega q2}^2 \tag{44}$$

According to the system (42), to find the differentiation of $V(e_{\omega q})$:

$$\begin{aligned} \dot{V}(e_{\omega q}) &= e_{\omega q1}\dot{e}_{\omega q1} + e_{\omega q2}\dot{e}_{\omega q2} \\ &= e_{\omega q1}e_{\omega q2} + e_{\omega q2}[-k_{\omega q1}e_{\omega q1} - k_{\omega q2}e_{\omega q2} - \tfrac{l}{\tan^{-1}(i_{qmax}^2 - i_q^2)}e_{\omega q2} - \overline{d}_{\omega q}] \\ &= -(k_{\omega q1} - 1)e_{\omega q1}e_{\omega q2} - [k_{\omega q2} + \tfrac{l}{\tan^{-1}(i_{qmax}^2 - i_q^2)}]e_{\omega q2}^2 - e_{\omega q2}\overline{d}_{\omega q} \\ &\leq -\tfrac{1}{2}(k_{\omega q1} - 1)\left(e_{\omega q1}^2 + e_{\omega q2}^2\right) - [k_{\omega q2} + \tfrac{l}{\tan^{-1}(i_{qmax}^2 - i_q^2)}]e_{\omega q2}^2 + \tfrac{1}{2}\left(e_{\omega q2}^2 + \overline{d}_{\omega q}^2\right) \\ &\leq -\tfrac{1}{2}(k_{\omega q1} - 1)e_{\omega q1}^2 - [\tfrac{k_{\omega q1}}{2} + k_{\omega q2} - 1 + \tfrac{l}{\tan^{-1}(i_{qmax}^2 - i_q^2)}]e_{\omega q2}^2 + \tfrac{1}{2}\overline{d}_{\omega q}^2 \end{aligned} \tag{45}$$

If the controller parameters $k_{\omega q1} > 1$ and $k_{\omega q2} > 1 - \frac{k_{\omega q1}}{2}$, then:

$$\dot{V}(e_{\omega q}) \leq -\beta_{k\omega q}V(e_{\omega q}) + \frac{1}{2}\overline{d}_{\omega q}^2 \tag{46}$$

where $\beta_{k\omega q}$ = min $\{k_{\omega q1}-1, k_{\omega q1} + 2k_{\omega q2}-2 + 2l/\tan^{-1}({i_{qmax}}^2-{i_q}^2)\}$ is a positive number.

At the moment, according to Lyapunov's theorem, (e_{wq1}, e_{wq2}) asymptotically converges Ω_E.

Next, according to Equation (42):

$$e_{\omega q2}\dot{e}_{\omega q2} = -k_{\omega q1}e_{\omega q1}e_{\omega q2} - k_{\omega q2}e_{\omega q2}^2 - \tfrac{l}{\tan^{-1}(i_{qmax}^2 - i_q^2)}e_{\omega q2}^2 - e_{\omega q2}\overline{d}_{\omega q} = F(e_{\omega q1}, e_{\omega q2}) \tag{47}$$

$F(e_{\omega q1}, e_{\omega q2})$ is a continuous function when $(-i_{qmax}, i_{qmax})$. If i_q approaches $\pm i_{qmax}$, $F(e_{\omega q1}, e_{\omega q2}) \to -\infty$. There is a constant $\bar{i}_{qmax} \in (0, i_{qmax})$, such that there must be $e_{\omega q2}\dot{e}_{\omega q2} < 0$ when $i_q \in [\bar{i}_{qmax}, i_{qmax}) \cup (-i_{qmax}, -\bar{i}_{qmax}]$, which means $|i_q| < i_{q\max}$ always hold. Thus, the inequality (45) is always true for any time.

Especially when $\bar{d}_{\omega q} = 0$, the closed loop system (41) is asymptotically stable at the equilibrium point. Meanwhile, $i_q(t) \in (-i_{qmax}, i_{qmax})$ always hold. □

5. Simulation Results

For the purpose of verifying the control performance and the effectiveness of the proposed method, a detailed simulation analysis was conducted by comparing it with different methods, which was performed by using MATLAB/Simulink. For the convenience of analysis, these methods are abbreviated as follows:

- 2PI: the conventional PI controller is employed in the speed and current double-loop.
- 2ADRC: the conventional ADRC is employed in the speed and current double-loop.
- 3PI: the conventional PI controller is employed in the position, speed, and current three-loop.
- 3ADRC: the conventional ADRC is employed in the position, speed, and current three-loop.
- 3ADRC1: the position loop ADRC of 3ADRC.
- Proposed method: ROADRC is employed in the position loop, and CACADRC is adopted for the integrated speed–current loop.

The EHA system parameters are detailed in Table 1 below.

Table 1. The EHA system parameters.

Parameters	Value
piston diameter of hydraulic cylinder (m)	0.066
piston rod diameter of hydraulic cylinder (m)	0.045
the piston stroke (m)	0.2
total leakage coefficient of hydraulic pump and cylinder($m^3/s{\cdot}Pa^{-1}$)	2×10^{-11}
effective oil bulk modulus (Pa)	6.86×10^8
the total volume of the hydraulic cylinder (m^3)	3×10^{-4}
the initial one-sided total volume of the hydraulic cylinder(m^3)	1.5×10^{-4}
the total viscous friction coefficient of the hydraulic cylinder and the load ($N/m{\cdot}s^{-1}$)	100
the total mass of the piston, piston rod, and load (kg)	60
displacement of the reversible plunger pump (m^3/rad)	1.5×10^{-6}
the viscous friction coefficient of the reversible piston pump ($N{\cdot}m/rad{\cdot}s^{-1}$)	0.002
PMSM-rated voltage (V)	380
PMSM-rated current (A)	7.6
PMSM-rated torque (N·m)	8
rotor flux linkage (Wb)	0.25
rotor inertia ($kg{\cdot}m^2$)	0.0012
the number of pole pairs	2
stator resistance (Ω)	1.1
the equivalent inductance (H)	0.0817
PMSM-rated rotating speed (rad/s)	550

5.1. Performance Simulation Analysis of CACADRC

In this simulation study, the speed tracking performance, disturbance rejection performance, and automatic current-constraint effectiveness of CACADRC are demonstrated. The current constraint is 16A, and the speed reference $\omega_{m\mathrm{d}}$ is 500 rad/s.

The simulation is divided into two cases. The first case is used to illustrate the current limiting effect of the current penalty coefficient l and provide guidance for choosing l.

The second case is used to compare the tracking performance and disturbance rejection performance of 2PI, 2ADRC, and CACADRC.

CACADRC parameters:

$\omega_{c\omega q}$ = 85 rad/s, $\omega_{o\omega q}$ = 5$\omega_{c\omega q}$; the control bandwidth of the current loop in *d*-axis is ω_{cd} = 1257 rad/s; and the ESO bandwidth is ω_{od} = 10ω_{cd}.

Case 1: Figure 4a–c shows ω_m, i_q and u_q response curves under the action of different current penalty coefficients *l*, respectively. It can be seen that i_q is constrained within the amplitude limit of 16A when l = 0.1$k_{\omega q2}$, $k_{\omega q2}$, and 2$k_{\omega q2}$, which means that the CACADRC can effectively realize automatic current-constraint control, and by adjusting the current penalty coefficient *l* in the barrier function, the current limiting intensity can be effectively adjusted. When *l* increases, the current i_q will decrease, resulting in a decrease in the response speed of ω_m. It should be noted that if the value of *l* is too large, the transient performance of the system will suffer a certain loss. On the contrary, if the value of *l* is too small, the current i_q will exceed the amplitude limit, which makes the circuit safety threatened. Therefore, a compromise should be considered in practical applications.

Figure 5a–c, respectively, shows ω_m, i_q and u_q response curves. To quantitatively analyze the performance of the different methods, the performance evaluation indices are employed, which are listed in Table 2, including overshoot (OS), settling time (ST), peak current (PC), speed drop (SD), recovery time (RT) and the number of parameters (PN).

2PI parameters:

Speed loop: $K_{P\omega}$ = 0.05, $K_{I\omega}$ = 0.3; *q*-axis current loop: K_{Pq} = 2.2, K_{Iq} = 564.8; *d*-axis current loop: K_{Pd} = 20, K_{Id} = 2011.

2ADRC parameters:

The control bandwidth of the speed loop is $\omega_{c\omega}$ = 21.4 rad/s, and the ESO bandwidth is $\omega_{o\omega}$ = 10$\omega_{c\omega}$; the control bandwidth of the current loop in the *d*-axis, *q*-axis is ω_{cd} = 1257 rad/s, ω_{cq} = 1257 rad/s, respectively; and the ESO bandwidth is ω_{od} = ω_{cd}, ω_{oq} = ω_{cq}, respectively.

CACADRC parameters:

Take l = 0.01 $k_{\omega q2}$, $\omega_{c\omega q}$ = 72 rad/s, $\omega_{o\omega q}$ = 10 $\omega_{c\omega q}$; ω_{cd} = 1257 rad/s, ω_{od} = 10 ω_{cd}.

Case 2: In the startup phase, it is observed in Figure 5a and Table 2 that, when compared with 2PI and 2ADRC, both CACADRC and 2ADRC can realize tracking without overshoot, while 2PI has a large overshoot. CACADRC and 2ADRC have the similar OS and ST, i.e., comparable tracking performance, which indicates that CACADRC does not need an excessive inner loop control bandwidth and requires fewer tuning parameters to have a similar dynamic performance as 2ADRC. In addition, in accordance with the requirement of i_q < 16A, it can be seen from Figure 5b and Table 2 that the i_q of 2PI, 2ADRC, and CACADRC are all kept within the current restricted range. The reason is that 2PI and 2ADRC constrain the current by limiting the control output $i_q{}^*$, while CACADRC constrains the current by adding the barrier function to the controller, which has the same current limiting effect as well as 2ADRC and 2PI.

An external load of 2000 N·m is suddenly applied at t = 1s. It can be seen from Figure 5a and Table 2 that CACADRC has a slightly better disturbance rejection ability than 2ADRC. While the 2PI has a larger SD and longer RT, that is, the disturbance rejection ability is poor. The reason is, on the one hand, the PI controller does not explicitly consider the speed regulation performance and disturbance rejection performance, it is to choose appropriate parameters to meet these performances in a compromise, while ADRC is a 2DOF controller, which can separately consider the speed regulation performance and disturbance rejection performance. On the other hand, the disturbance rejection effect of the PI controller is mainly realized by the integration effect, and the integration has a cumulative effect, so the disturbance compensation will inevitably be delayed. Although the delay effect can be alleviated by increasing the integral gain of the controller, a large integral gain will lead to a larger overshoot of the step response when there is no external load.

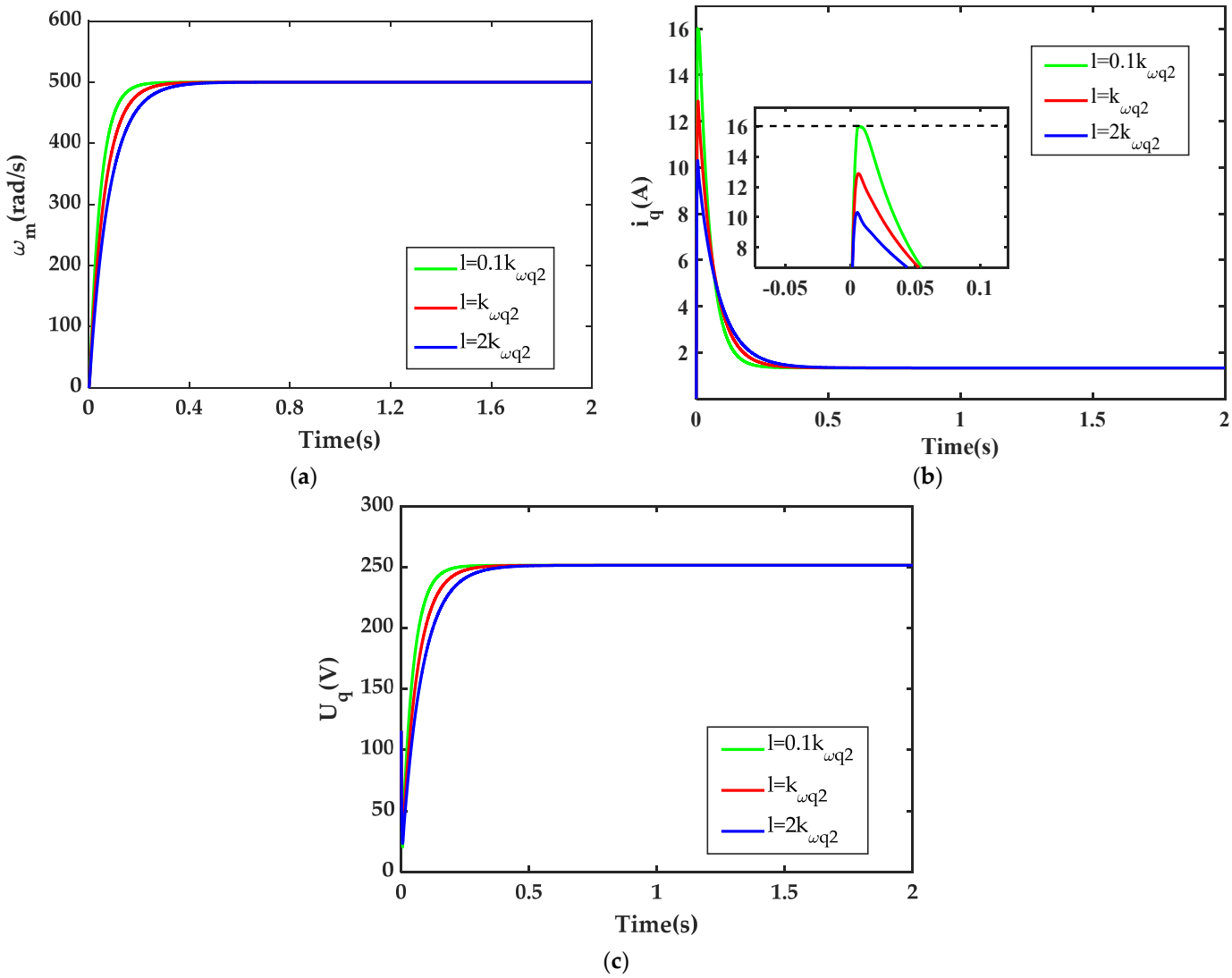

Figure 4. Performance comparisons under CACADRC with different current penalty coefficients *l*. (**a**) Speed response curves; (**b**) *q*-axis current response curves; and (**c**) *q*-axis voltage response curves.

Table 2. Performance evaluation indices.

Performance	OS (%)	ST (s)	PC (A)	SD (rad/s)	RT (s)	PN
2PI	9	0.78	16	32	0.64	6
2ADRC	0	0.45	16	11	0.27	6
CACADRC	0	0.4	16	5.5	0.13	5

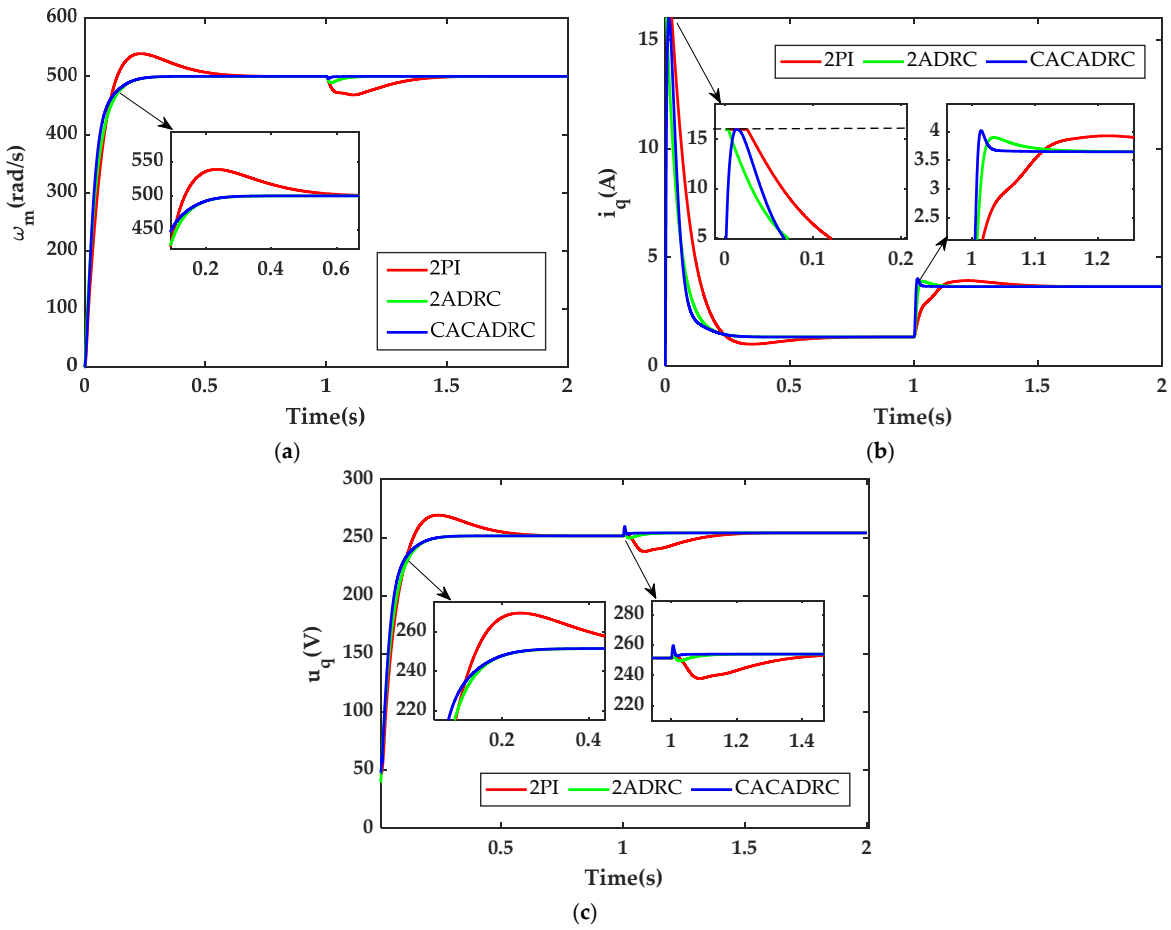

Figure 5. Speed step response comparison curves with ω_{md} = 500 rad/s. (**a**) Speed response curves; (**b**) q-axis current response curves; and (**c**) q-axis voltage response curves.

5.2. Performance Simulation Analysis of ROADRC

In this simulation study, the position tracking performance, disturbance rejection performance, and ESO noise reduction effect of ROADRC are demonstrated.

The simulation is divided into two cases. The first case is the position tracking performance, disturbance rejection performance, and sensitivity to noise of 3PI, 3ADRC, and the proposed method when the position reference is a step signal. The second case is the position tracking performance, disturbance rejection performance, and sensitivity to noise of 3PI, 3ADRC, and the proposed method when the position reference is a time-varying signal.

3PI parameters: Position loop: K_{Px} = 12661.58, K_{Ix} = 48091.89. $K_{P\omega}$ = 0.05, $K_{I\omega}$ = 0.3; K_{Pq} = 2.2, K_{Iq} = 564.8; K_{Pd} = 20, K_{Id} = 2011.

3ADRC parameters:

The control bandwidth of 3ADRC1 is ω_{cx} = 94 rad/s, and the ESO bandwidth is ω_{ox} = 10 ω_{cx}. $\omega_{c\omega}$ = 628 rad/s, $\omega_{o\omega}$ = 5 $\omega_{c\omega}$; ω_{cd} = 1257 rad/s, ω_{cq} = 1257 rad/s; ω_{od} = ω_{cd}, ω_{oq} = ω_{cq}.

The proposed method parameters:

Take l = 19 $k_{\omega q2}$, ω_{cx} = 94 rad/s, ω_{ox} = 10 ω_{cx}; $\omega_{c\omega q}$ = 628 rad/s, $\omega_{o\omega q}$ = 5 $\omega_{c\omega q}$; ω_{cd} = 1257 rad/s, ω_{od} = ω_{cd}.

Case 1: The position reference x_d is 0.1m, and a uniformly distributed noise signal with an amplitude of 1×10^{-5} is added to the position signal x. The comparison curves of position step performance are shown in Figure 6. As shown in Figure 6a, it is seen that although 3PI has the fastest response speed, it produces a 10% overshoot, while the proposed method and 3ADRC achieve almost the same tracking performance without overshoot.

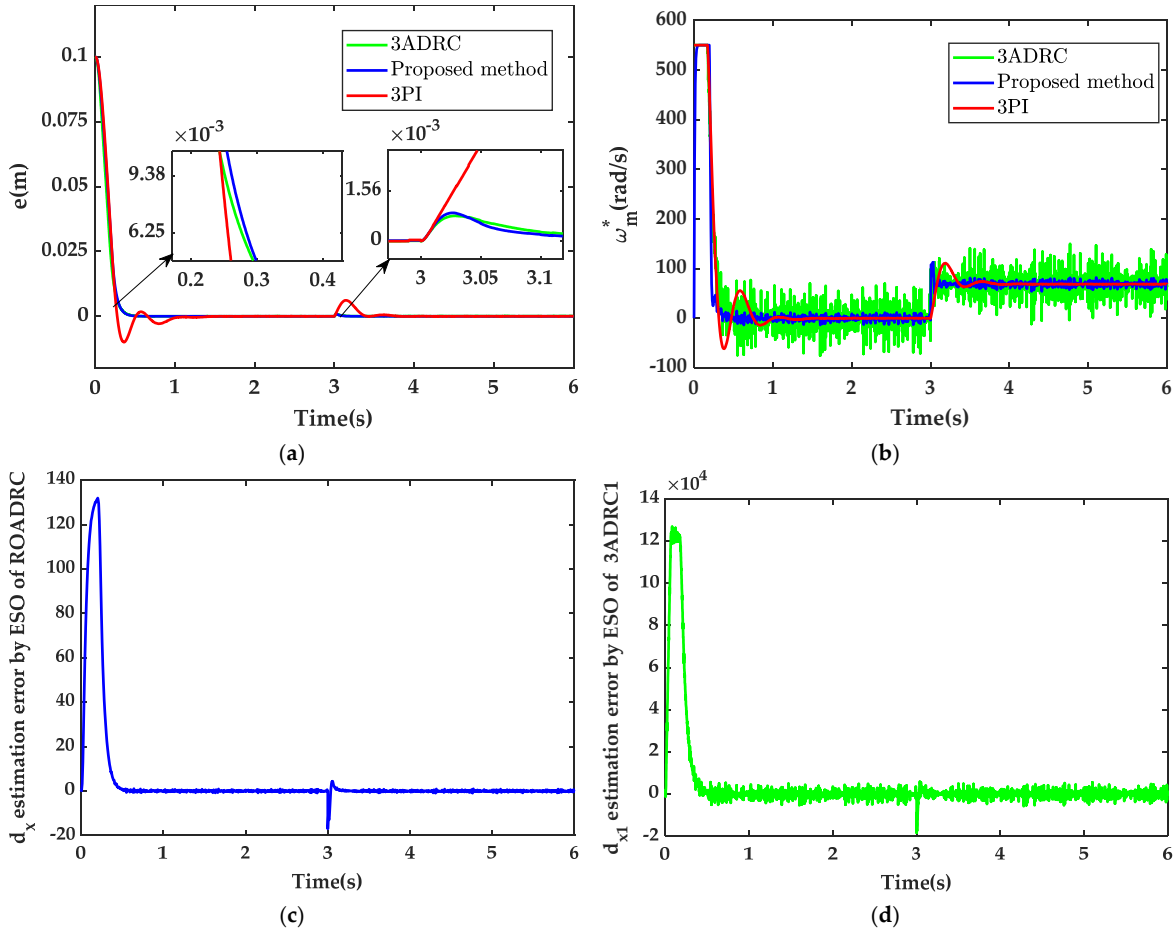

Figure 6. Position step response comparison curves with x_d = 0.1m. (**a**) Comparison curves of position tracking errors of 3ADRC, the proposed method and 3PI; (**b**) control output $\omega_m{}^*$ response curves; (**c**) disturbance estimation error by ESO of ROADRC; and (**d**) disturbance estimation error by ESO of 3ADRC1.

The external load force of 1000 N is suddenly applied at t = 3 s. It can be seen from Figure 6a that the 3PI produces a position error of about 0.0062 m, and the position recovery time is about 0.84 s. Although 3PI can recover to its original position eventually, the recovery time is very long, while 3ADRC produces a position error of about 0.0012 m with a position recovery time of about 0.35 s, and the proposed method produces a position error of about 0.001 m with a position recovery time of about 0.35 s. It can be seen that the proposed method and 3ADRC have similar disturbance rejection capabilities, because both of them estimate and compensate for the disturbance in real-time through ESO, while the disturbance rejection ability of 3PI is significantly worse than that of 3ADRC and the proposed method because PI controller is used to suppress the disturbance through integration.

Moreover, it can be calculated:

The disturbance quantity d_x of ROADRC:

$$d_x = F_L/m_t = -16.7 \tag{48}$$

The disturbance quantity d_{x1} of 3ADRC1:

$$d_{x1} = \beta_e C_t (m_t V_0)^{-1} F_L = -1.5 \times 10^4 \tag{49}$$

Figure 6c,d shows that the ESO to disturbance estimation curve of ROADRC is smoother than that of 3ADRC1 because the ESO order of ROADRC is lower than that

of 3ADRC1, in other words, the disturbance estimation of ROADRC is more accurate than that of 3ADRC1.

In addition, it can be seen from Figure 6b that the control output $\omega_m{}^*$ of 3ADRC1 is more seriously polluted by noise than that of ROADRC. The reason is the ESO order of 3ADRC1 is one order higher than that of ROADRC, so it is sensitive to noise, and the 3ADRC1 introduces the actuation acceleration information, which has an amplification effect on noise. However, the control output curve $\omega_m{}^*$ of the position loop PI is the smoothest, because only the proportional term of the position loop PI introduces noise, and the integral term can suppress the noise to a certain extent.

Case 2: The position reference x_d is 0.001 sin ($4\pi t$) m, and a uniformly distributed noise signal with an amplitude of 1×10^{-5} is added to the position signal x. In order to verify the influence of interference force and parameter mutation on system performance, it is assumed that external load F_L = 500 sin ($2\pi t$) N is applied at t = 0 s, while total mass of the piston, piston rod and load m_t and total leakage coefficient of the pump and the hydraulic cylinder C_t become twice the original value, respectively.

The comparison curves of position tracking performance are manifested in Figure 7. It can be seen from Figure 7a that 3PI has the largest tracking error, and the tracking error of ROADRC is slightly smaller than that of 3ADRC, which indicates that the disturbance rejection ability of the proposed method is slightly better than that of 3ADRC and significantly better than that of 3PI. As can be seen from Figure 7c,d, the disturbance estimation error curve of ROADRC's ESO is smoother than that of 3ADRC1, since the ESO order of ROADRC is lower than that of 3ADRC1. In addition, it can be indicated from Figure 7b that the control output $\omega_m{}^*$ of 3ADRC1 is more seriously polluted by noise than that of ROADRC.

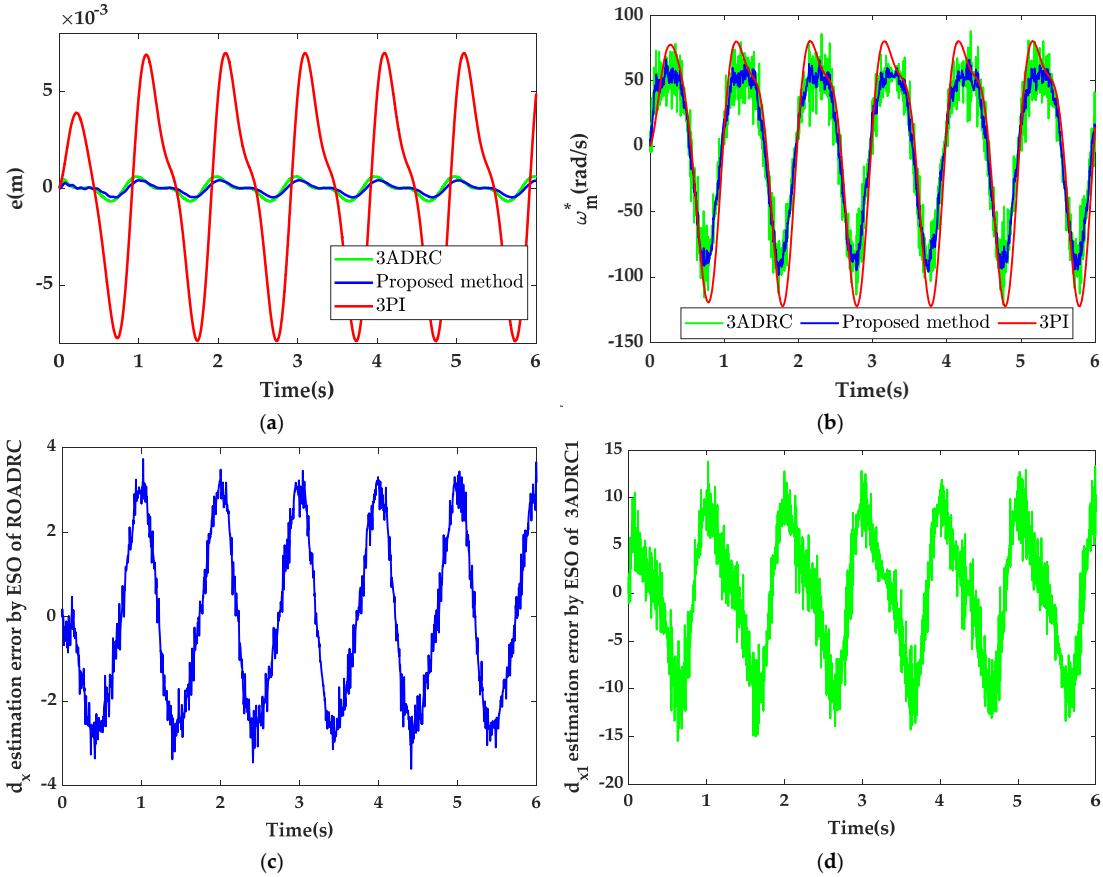

Figure 7. Position time-varying signal response comparison curves under complex disturbance when x_d = 0.001 sin ($4\pi t$) m. (**a**) Comparison curves of position tracking errors of 3ADRC, the proposed

method and 3PI; (**b**) control output $\omega_m{}^*$ response curves; (**c**) disturbance estimation error by ESO of ROADRC; and (**d**) disturbance estimation error by ESO of 3ADRC1.

6. Conclusions

In this paper, a novel cascade double-loop ADRC control architecture, including the reduced order position control loop and an integrated speed–current control loop, was proposed to improve the control performance of EHA. By comparing with traditional three-loop PI controller and traditional three-loop ADRC, the following conclusions can be given:

1. The barrier function introduced in CACADRC can effectively achieve automatic current-constraint control, and by adjusting the current penalty coefficient l in the barrier function, the current limiting intensity can be effectively adjusted. Compared with 2PI and 2ADRC, both CACADRC and 2ADRC can realize tracking without overshoot, while 2PI has a large overshoot. In terms of anti-disturbance ability, CACADRC and 2ADRC have a more excellent anti-disturbance performance than 2PI, and CACADRC has a slightly better anti-disturbance ability than 2ADRC.
2. When the position reference is a step signal, both the proposed method and 3ADRC can achieve tracking without overshoot, while 3PI has a large overshoot. Moreover, the disturbance rejection performance of the proposed method is similar to that of 3ADRC and superior to that of 3PI when subjected to step disturbance. In addition, when the position reference is a sinusoidal time-varying signal, the disturbance rejection ability of the proposed method is slightly better than that of 3ADRC and significantly better than that of 3PI.
3. Due to the reduced order processing of the position subsystem, the order of the ESO of ROADRC is lower than that of the ESO of 3ADRC1, and the noise sensitivity is effectively weakened, which makes the disturbance estimation of the ROADRC's ESO smoother than that of 3ADRC1. Moreover, in the process of ROADRC design, the use of acceleration information is avoided, so the control output signal $\omega_m{}^*$ of ROADRC is smoother than that of 3ADRC1.
4. The proposed novel cascaded double-loop ADRC control architecture is simpler than the traditional cascaded three-loop ADRC control architecture and requires fewer parameters to be tuned, which is more conducive to the application in practical engineering.

Author Contributions: Conceptualization, R.Y., Y.M. and L.Z.; methodology, R.Y. and Y.M.; software, R.Y. and Y.M.; validation, R.Y., Y.M. and L.Z.; formal analysis, Y.M., L.Z. and H.H.; investigation, J.Z.; resources, H.H.; data curation, L.Z. and H.H.; writing—original draft preparation, R.Y. and Y.M.; writing—review and editing, R.Y., Y.M., J.Z. and L.Z.; visualization, R.Y., L.Z. and J.Z.; supervision, J.Z., L.Z. and H.H.; project administration, J.Z. All authors have read and agreed to the published version of the manuscript.

Funding: This research was funded by the National Natural Science Foundation of China (grant number: 51565030) and the Science and Technology Program of Gansu Province (grant number: 20JR10RA175).

Institutional Review Board Statement: Not applicable.

Informed Consent Statement: Informed consent was obtained from all subjects involved in the study.

Data Availability Statement: Not applicable.

Acknowledgments: The authors acknowledge the English review process conducted by MDPI services.

Conflicts of Interest: The authors declare no conflict of interest.

Nomenclature

Symbol	Comment
EHA	electro-hydrostatic actuator
ADRC	active disturbance rejection control
ESO	extended state observer
ROADRC	reduced-order ADRC controller
CACADRC	automatic current-constrained ADRC controller
PI	proportional integral controller
2DOF	two-degree-of-freedom
RISE	the robust integral of the sign of error
PMSM	permanent magnet synchronous motor
u_q, u_d	q, d axis voltage components
R_h	stator resistance
i_g, i_d	q, d axial current components
L_q, L_d	the equivalent inductance of q, d axis
ω_m	the mechanical angular speed of PMSM
p	the number of pole pairs
ψ_f	flux linkage of the rotor permanent magnet
J_p	rotor inertia
B_p	the coefficient of viscous friction of the reversible plunger pump
D_p	displacement of the reversible plunger pump
p_a, p_b	oil outlet and inlet pressures of the pump
Q_a, Q_b	oil outlet and inlet flow of the pump
Q_{ip}, Q_{opa}, Q_{opb}	internal and external leakage flow of the pump
β_e	effective oil bulk modulus
V_a, V_b	volumes of the oil outlet chamber and oil return chamber of the pump
Q_1, Q_2	inflow and outflow flow of the two chambers of the hydraulic cylinder
A	the effective working area of the hydraulic cylinder piston
x	displacement of the piston rod of the hydraulic cylinder
p_1, p_2	the pressure of the two chambers of the hydraulic cylinder
Q_{ic}	internal leakage flow in the hydraulic cylinder
V_{10}, V_{20}	volumes of the closed chamber on both sides of the hydraulic cylinder
m_t	the total mass of the piston, piston rod, and load
B_t	the total viscous friction coefficient of the hydraulic cylinder and the load
F_L	the external load force applied to the piston rod
Q_{c1}, Q_{c2}	flow through the check valve
Q_{r1}, Q_{r2}	flow through the relief valve
p_L	load pressure
C_t	total leakage coefficient of the pump and the hydraulic cylinder
$\overline{p}_L$	quasi-steady state quantity
ω_{mc}	disturbance compensation control quantity of ROADRC
ω_{m0}	nominal control quantity of ROADRC
ω_{m*}	control output of ROADRC
l_{x1}, l_{x2}, l_{x3}	ESO gains of ROADRC
X_d	position reference
k_{x1}, k_{x2}	control parameters of ROADRC
ω_{ox}	ESO bandwidth of the position loop
ω_{cx}	control bandwidth of the position loop
u_{qc}	disturbance compensation control quantity of the integrated speed–current control
u_{q0}	nominal control quantity of the integrated speed–current control
u_{qi*}	the output of the integrated speed–current control
$l_{\omega q1}$, $l_{\omega q2}$, $l_{\omega q3}$	ESO gains of the integrated speed–current control
ω_{md}	speed reference
$k_{\omega q1}$, $k_{\omega q2}$	control parameters of the integrated speed–current controller
u_{q*}	control output of CACADRC
f_{br}	barrier function

l	current penalty coefficient
i_{qmax}	limiting value of i_q
$\omega_{o\omega q}$	ESO bandwidth of CACADRC
$\omega_{c\omega q}$	control bandwidth of CACADRC
2PI	the conventional PI controller is employed in the speed and current double-loop
2ADRC	the conventional ADRC is employed in the speed and current double-loop
3PI	the conventional PI controller is employed in the position, speed, and current three-loop
3ADRC	the conventional ADRC is employed in the position, speed, and current three-loop
3ADRC1	the position loop ADRC of 3ADRC
Proposed method	ROADRC is employed in the position loop, and CACADRC is adopted for the integrated speed–current loop
ω_{cd}	control bandwidth of the current loop in the d-axis
ω_{od}	ESO bandwidth of the current loop in the d-axis
D	piston diameter of the hydraulic cylinder
d	piston rod diameter of hydraulic cylinder
L	piston stroke
V	the total volume of the hydraulic cylinder
V_0	the initial one-sided volume of the hydraulic cylinder
u_{N}	PMSM-rated voltage
I_{N}	PMSM-rated current
T_{N}	PMSM-rated torque
ω_{mN}	PMSM-rated rotating speed
OS	overshoot
ST	settling time
PC	peak current
SD	speed drop
RT	recovery time
PN	number of parameters
$K_{P\omega}$, $K_{I\omega}$	proportion and integral gains of speed loop of 2PI
K_{Pq}, K_{Iq}	proportion and integral gains of the q-axis current loop of 2PI
K_{Pd}, K_{Id}	proportion and integral gains of the d-axis current loop
$\omega_{c\omega}$	control bandwidth of the speed loop of 2ADRC
$\omega_{o\omega}$	ESO bandwidth of the speed loop of 2ADRC
ω_{cq}	control bandwidth of the current loop in the q-axis of 2ADRC
ω_{oq}	ESO bandwidth of the current loop in the q-axis of 2ADRC
K_{Px}, K_{Ix}	proportion and integral gains of the position loop of 3PI
ω_{cx}	control bandwidth of the position loop
ω_{ox}	ESO bandwidth of the position loop
d_x	disturbance quantity of ROADRC
d_{x1}	disturbance quantity of 3ADRC1

References

1. Fu, Y.L.; Han, X.; Yang, R.R.; Qi, H.T.; Fu, J. Review on Design Method of Electro-hydrostatic Actuator. *J. Beijing Univ. Aeronaut. Astronaut.* **2017**, *43*, 1939–1952. (In Chinese) [CrossRef]
2. Mare, J.C.; Fu, J. Review on Signal-by-Wire and Power-by-Wire Actuation for More Electric Aircraft. *Chin. J. Aeronaut.* **2017**, *30*, 857–870. [CrossRef]
3. Alle, N.; Hiremath, S.S.; Makaram, S.; Subramaniam, K.; Talukdar, A. Review on Electro-hydrostatic Actuator for Flight Control. *Int. J. Fluid Power* **2016**, *17*, 125–145. [CrossRef]
4. Ko, T.; Murotani, K.; Yamamoto, K.; Nakamura, Y. Whole-Body Compliant Motion by Sensor Integration of an EHA-Driven Humanoid Hydra. *Int. J. Hum. Robot.* **2021**, *18*, 2150002. [CrossRef]
5. Kou, F.R. The Control Study of Vehicle Active Suspension with Electro-hydrostatic Actuator. *Appl. Mech. Mater.* **2011**, *97–98*, 716–720. [CrossRef]
6. Sun, W.C.; Gao, H.J.; Yao, B. Adaptive Robust Vibration Control of Full-Car Active Suspensions with Electro-hydraulic Actuators. *IEEE Trans. Control Syst. Technol.* **2013**, *21*, 2417–2422. [CrossRef]

7. Chiang, M.H.; Chen, C.C.; Kuo, C.F.J. The High Response and High Efficiency Velocity Control of a Hydraulic Injection Molding Machine Using a Variable Rotational Speed Electro-hydraulic Pump-Controlled System. *Int. J. Adv. Manuf. Technol.* **2009**, *43*, 841–851. [CrossRef]
8. Ahn, K.K.; Nam, D.N.C.; Jin, M. Adaptive Backstepping Control of an Electro-hydraulic Actuator. *IEEE/ASME Trans. Mechatron.* **2013**, *19*, 987–995. [CrossRef]
9. Lee, W.; Kim, M.J.; Chung, W.K. Asymptotically Stable Disturbance Observer-Based Compliance Control of Electro-hydrostatic Actuators. *IEEE/ASME Trans. Mechatron.* **2019**, *25*, 195–206. [CrossRef]
10. Li, L.J.; Wang, M.K.; Yang, R.R.; Fu, Y.L.; Zhu, D.M. Adaptive Damping Variable Sliding Mode Control for an Electro-hydrostatic Actuator. *Actuators* **2021**, *10*, 83. [CrossRef]
11. Ge, Y.W.; Yang, X.W.; Deng, W.X.; Yao, J.Y. Rise-Based Composite Adaptive Control of Electro-hydrostatic Actuator with Asymptotic Stability. *Machines* **2021**, *9*, 181. [CrossRef]
12. Wang, Y.; Wang, M.K.; Fu, J.; Fu, Y.L. Adaptive Control of an Aerospace Electro-hydrostatic Actuator with a Constant-Torque Variable-Displacement Pump. *J. Aerosp. Eng.* **2022**, *35*, 04022028. [CrossRef]
13. Han, J.Q. From PID to Active Disturbance Rejection Control. *IEEE Trans. Ind. Electron.* **2009**, *56*, 900–906. [CrossRef]
14. Gao, Z.Q.; Huang, Y.; Han, J.Q. An Alternative Paradigm for Control System Design. In Proceedings of the 40th IEEE Conference on Decision and Control, Orlando, FL, USA, 4–7 December 2001; pp. 4578–4585. [CrossRef]
15. Wang, Y.C.; Fang, S.H.; and Hu, J.X. Active Disturbance Rejection Control based on Deep Reinforcement Learning of PMSM for More Electric Aircraft. *IEEE Trans. Power Electron.* **2023**, *38*, 406–416. [CrossRef]
16. Zhu, L.H.; Zhang, G.Q.; Jing, R.Z.; Bi, G.D. Nonlinear Active Disturbance Rejection Control Strategy for Permanent Magnet Synchronous Motor Drives. *IEEE Trans. Energy Convers.* **2022**, *37*, 2119–2129. [CrossRef]
17. Xu, Z.B.; Deng, W.X.; Shen, H.; Yao, J.Y. Extended-State-Observer-Based Adaptive Prescribed Performance Control for Hydraulic Systems with Full-State Constraints. *IEEE/ASME Trans. Mechatron.* **2022**, 1–11. [CrossRef]
18. Liu, C.; Yue, X.K.; Zhang, J.Q.; Shi, K.K. Active Disturbance Rejection Control for Delayed Electromagnetic Docking of Spacecraft in Elliptical Orbits. *IEEE Trans. Aerosp. Electron. Syst.* **2022**, *58*, 2257–2268. [CrossRef]
19. Xu, L.X.; Ma, H.J.; Guo, D.; Xie, A.H.; Song, D.L. Backstepping Sliding-Mode and Cascade Active Disturbance Rejection Control for a Quadrotor UAV. *IEEE/ASME Trans. Mechatron.* **2020**, *25*, 2743–2753. [CrossRef]
20. Lara-Ortiz, V.; Guarneros, A.; Llorente-Vidrio, D.; Cruz-Ortiz, D.; Salgado, I.; Chairez, I. Active Disturbance Rejection Controller for a Flexible Walking Bioinspired Inchworm Mobile Robot Actuated with Shape Memory Alloy Devices. *IEEE Trans. Control Syst. Technol.* **2022**, *30*, 1790–1797. [CrossRef]
21. Blas, L.A.; Dávila, J.; Salazar, S.; Bonilla, M. Robust Trajectory Tracking for an Uncertain UAV Based on Active Disturbance Rejection. *IEEE Control Syst. Lett.* **2022**, *6*, 1466–1471. [CrossRef]
22. Han, X.X.; Chen, Z.X.; Feng, Y.B.; Xie, J.; Wei, X.L.; Wei, L.J. Cascade Active Disturbance Rejection Control of Single-Rod Electro-hydrostatic Actuator. *Asian J. Control* **2022**, 1–17. [CrossRef]
23. Yang, R.R. Research on Control Strategy for Electro-Hydrostatic Actuation System Based on a Novel Integrated Electro-hydraulic Pump. Ph.D. Thesis, Beijing University of Aeronautics and Astronautics, Beijing, China, 2019; pp. 76–77. (In Chinese)
24. Wang, M.K.; Wang, Y.; Fu, Y.L.; Yang, R.R.; Zhao, J.A.; Fu, J. Experimental Investigation of an Electro-hydrostatic Actuator based on the Novel Active Compensation Method. *IEEE Access* **2020**, *8*, 170635–170649. [CrossRef]
25. Khalil, H.K. *Nonlinear Systems*, 3rd ed.; Pearson Education: Hoboken, NJ, USA, 2002; pp. 423–430.
26. Gao, Z.Q. Scaling and Bandwidth-Parameterization based Controller Tuning. In Proceedings of the American Control Conference, Denver, CO, USA, 4–6 June 2003; pp. 4989–4996. [CrossRef]